



Article

Forbidden Reflections in TeO₂ in the Vicinity of the Te L₁ Absorption Edge

Elena Ovchinnikova ¹, Dmitri Novikov ², Matthias Zschornak ³, Anton Kulikov ⁴, Ksenia Kozlovskaya ^{1,*}, Vladimir Dmitrienko ⁴, Alexey Oreshko ¹, Alexander Blagov ⁵, Enver Mukhamedzhanov ⁵, Nikita Marchenkov ⁵, Mikhail Borisov ⁵, Azat Khadiev ², Arsen Petrenko ⁵ and Yuri Pisarevsky ⁴

¹ Physics Department of Moscow State University, 119899 Moscow, Russia; en_ovchinnikova@physics.msu.ru (E.O.); oreshko@mail.ru (A.O.)

² Deutsches Elektronen-Synchrotron DESY, Notkestraße 85, 22607 Hamburg, Germany; dmitri.novikov@desy.de (D.N.); azat.khadiev@desy.de (A.K.)

³ Institute of Experimental Physics, TU Bergakademie Akademiestraße 6, 09599 Freiberg, Germany; matthias.zschornak@physik.tu-freiberg.de

⁴ A.V. Shubnikov Institute of Crystallography, FSRC “Crystallography and Photonics” RAS, Leninskiy Prospekt, 59, 119333 Moscow, Russia; ontonic@gmail.com (A.K.); dmitrien@crys.ras.ru (V.D.); yupisarev@yandex.ru (Y.P.)

⁵ National Research Center “Kurchatov Institute”, Ploshchad’ Akademika Kurchatova, 1, 123098 Moscow, Russia; blagov_ae@nrcki.ru (A.B.); mukhamedzhanov@gmail.com (E.M.); marchenkov_nv@mail.ru (N.M.); borisov.kcsr@gmail.com (M.B.); diacon0301@gmail.com (A.P.)

* Correspondence: kozlovskaya@physics.msu.ru; Tel.: +7-916-805-60-90

Received: 8 July 2020; Accepted: 8 August 2020; Published: 19 August 2020



Abstract: Examining forbidden reflections provides valuable information on electronic states and the local environment of resonant atoms in crystals. Experimental studies of two forbidden reflections 002 and 100 in TeO₂ single crystals were performed at photon energies close to the L₁ tellurium absorption edge. It was found that the spectral form corresponding to these two reflections looks almost identical, which is completely unexpected for a highly anisotropic material. Theoretical consideration shows that only one component f_{xy} of the tensor describing dipole-dipole resonance scattering contributes to the 002 reflection, while two components f_{xy} and f_{xz} correspond to the 100 reflection. Numerical calculations show that the latter tensor component is comparable to the first one, but the combination of several geometric factors leads to the fact that its contribution to the spectrum is negligible. This explains the experimentally observed results. The finding shows a way for targeted investigation of single tensor components and makes it possible to compare different spectra and use them to study the physical phenomena in functional materials.

Keywords: X-ray resonant diffraction; forbidden reflections; X-ray spectroscopy

1. Introduction

The study of the properties of functional materials is an important goal of condensed matter physics, and increasingly sophisticated physical methods are being developed for its implementation. Synchrotron radiation allows to investigate structural, magnetic, electronic and other properties of a solid at high resolution due to its unique properties, such as high brightness, wide energy spectrum, polarization, etc., including coherence available in fourth generation sources. Resonant X-ray diffraction is a method that resolves these properties of crystals locally at the atomic level [1]. Forbidden reflections appearing in crystals at incident radiation energy near the absorption edges [2,3] are particularly sensitive, as the complex three-dimensional information can be extracted from

energy spectra, azimuthal and polarization properties of X-ray reflections [4]. Contrary to the DAFS method [5,6], where the spectra of allowed Bragg reflections are studied, in the forbidden Bragg reflections any contribution from non-resonant Thomson scattering is absent making subtle resonant scattering more pronounced. In numerous studies of forbidden reflections, the great possibilities of the method were demonstrated using examples of determining the magnetic structure [7–9], orbital and charge ordering [10,11], local chirality [12,13] and thermal displacements of atoms [14–17] etc. Particularly exciting is the opportunity to study variations of local properties when the crystal is exposed to external influences. The subject of investigation up to now was mostly the influence of magnetic field and temperature on forbidden reflections. However an external electric field can also cause structural changes in crystals [18,19].

This was demonstrated, for example, in a study of allowed resonant diffraction in KDP [20]. Indeed, the symmetry of many functional materials is described by symmorphic space groups, hence no forbidden reflections exist. In [21], promising method was proposed, which uses allowed but weak reflections at the energies of incident radiation close to an absorption edge. Using this method the formation of a new polar phase in cubic SrTiO₃ due to an applied electric field was observed. This phase transition is a result of oxygen vacancies migration, and the mechanism paves the way for managing the physical properties of materials. Structural changes observed in paratellurite TeO₂ in applied electric field [22–25] also are associated with oxygen vacancy migration. Contrary to SrTiO₃, the TeO₂ crystal intrinsically possesses piezoelectric properties and its symmetry is described by a non-symmorphic space group, which provides a set of forbidden reflections in the reciprocal space. It would be interesting to study the evolution of the forbidden reflections properties in piezoelectric material under applied electric field. In opposite to the study of weak, but non-forbidden reflection in [21], appearance of the forbidden reflections is associated with anisotropic polarization dependent part of resonant structure factor while the isotropic part of scattering is zero. This anisotropic part in general is determined by several tensor components. Different tensor components give different contributions and different reflections and can react differently to external influences. Therefore at first it is necessary to study the properties of the forbidden reflections in TeO₂ without external influence aiming to choose the optimal conditions for future investigations. The present work is devoted to theoretical and experimental study of two kinds of forbidden reflections 00*l* with $l = 4n + 2$ and *h*00 with $h = 2n + 1$ in TeO₂ in the vicinity of the *L*₁ absorption edge. According to previous research carried out on a laboratory source, *h*00 reflections are more sensitive to the applied electric field. In this paper, it is shown that two tensor components determine the spectral shape of forbidden reflections of this type. Since external influences can change tensor components in different ways, the presence of two components can complicate the interpretation of the results. The experimentally found similarity of the 002 and 100 reflections energy spectra made it possible to establish that one of the tensor components contributing to the 100 reflection is small. From this point of view, reflection 100, for which one tensor component can be neglected due to its smallness, is quite suitable for further research with electric field. On the other hand, the study of tensor components is of interest in itself, since they characterize electronic states excited due to the dipole resonant transitions close to the *L*₁ edge of Te. In this work, it is shown that experimental data in combination with theoretical calculations make it possible to determine the ratio of two tensor components describing the resonance part of the atomic factor of tellurium.

2. Symmetry Analysis of Resonant X-Ray Scattering

When the energy of incident synchrotron radiation is close to an absorption edge of an atom, the resonant X-ray scattering appears and the scattering amplitude corresponding to any Bragg reflection can be represented as a sum:

$$F(\mathbf{H}) = F_0(\mathbf{H}) + F_{ij}^{res}(\mathbf{H}, E), \quad (1)$$

where $F_0(\mathbf{H})$ describes conventional Thomson scattering of X-rays and $F_{ij}^{res}(\mathbf{H}, E)$ is the resonant contribution. The latter contains isotropic real and imaginary parts widely known as dispersion corrections, but sometimes it also includes anisotropic parts, usually described in terms of multipolar transitions between the inner electronic shell and excited states. In the Cartesian representation, it leads to a superposition of tensors of various ranks [26]:

$$f'_{jk} + if''_{jk} \sim D_{jk} - \frac{i}{2}(k_m I_{jkm} - k'_m I_{kjm}^*) + \frac{1}{4}k'_m k_n Q_{jkmn}, \quad (2)$$

where the summation over repeated indices is implied. In non-magnetic TeO_2 crystals, the resonant scattering tensor consists only of the second rank dipole-dipole E1E1 tensor D , the third rank dipole-quadrupole tensor I , and the fourth rank quadrupole-quadrupole tensor Q . The tensor components of all the tensors have complex values depending on the X-ray energy. The higher is a rank of the multipole transition the weaker is its contributions to the resonant scattering factor.

In nonmagnetic crystals, anisotropic resonant scattering occurs due to the splitting of electronic levels in a crystalline field, so that this contribution is unique and depends not only on the chemical composition and electronic state of the crystal but also on the Wyckoff position occupied by the resonant atom. In those cases when $F(\mathbf{H}) = 0$ due to the glide-plane or screw-axes extinction laws, but $F_{ij}^{res}(\mathbf{H}, E) \neq 0$ the so-called “forbidden” reflections can appear at the photon energies close to the absorption edges of atoms. Since their theoretical prediction [2] and first observation [5,6] various kinds of such reflections were observed in crystals associated with various multipole resonant contributions to the atomic factor. The integrated intensity of forbidden reflections is small compared with the conventional Bragg reflections, therefore they often are masked by the Renninger multiple reflections, which appear at certain azimuthal angles. Therefore, it is possible to separate resonant scattering from multiple scattering rotating a sample around the scattering vector.

As the interaction of the electromagnetic wave in the forbidden scattering channel is rather weak, it is usually described by the kinematical theory of diffraction. In this approximation, the following expression can be applied to calculate an integrated intensity in the Bragg geometry [26]:

$$I(hkl) \sim \frac{|F(E, \mathbf{H})|^2 [1 - \exp^{-(\frac{\mu_{in}}{\sin \alpha} + \frac{\mu_{out}}{\sin \beta})t}]}{\mu_{in}(E) + \mu_{out} \frac{\sin \alpha}{\sin \beta}}, \quad (3)$$

where t is the crystal thickness, $\mu_{in}(E)$ and $\mu_{out}(E)$ are the absorption coefficient, corresponding to the incoming and outgoing waves, α and β describe the angles of incidence and exit of the X-ray beam with respect to the crystal surface. In the symmetric Bragg geometry $\frac{\sin \alpha}{\sin \beta} = 1$. $F(E, \mathbf{H})$ is the structure amplitude, which is a sum over all atoms inside a unit cell:

$$F(E, \mathbf{H}) = \sum_s f_{ij}^s(E, \mathbf{H}) \exp(-M_s) \exp(i\mathbf{H}\mathbf{r}_s), \quad (4)$$

$f_{ij}^s(E, \mathbf{H})$ is the atomic factor of the atom s , \exp^{-M_s} – Debye-Waller factor. $M_s = \frac{1}{2}\langle(\mathbf{H} \cdot \mathbf{u}_s)^2\rangle$, \mathbf{u}_s is at atomic displacement. It is worth to raise the question whether it possible to consider $\mu_{in} = \mu_{out}$. Because the forbidden reflections exist in the vicinity of absorption edges, in this region the absorption coefficient $\mu(E)$ also contains the resonant part, which can be anisotropic giving rise to linear dichroism [27]. In principle linear polarizations are not the eigen vectors in anisotropic media, this is well known for visible light optics. This question was also studied in details in scientific works devoted to the diffraction of Mössbauer radiation in crystals [28,29]. However the anisotropy in Mössbauer diffraction is very strong, while in X-ray resonant diffraction it is rather weak. For this reason, the anisotropy of absorption is usually neglected in the calculation of forbidden reflections intensity.

The coefficients f_{ij} are complex values and in the dipole-dipole approximation can be calculated as a sum over all electrons:

$$f'_{ij} + if''_{ij} = \frac{m}{\hbar^3 \omega} \sum_{f,g} (E_f - E_g)^3 \frac{\langle g | R_i | f \rangle \langle f | R_j | g \rangle}{\hbar \omega - (E_f - E_g) - i\Gamma/2} \quad (5)$$

where E_g and E_f are the energies of the ground g and excited f states, Γ is the width of the excited state, also depending on E . In the dipole transition operator of the electric field $R_j = \sum_j \mathbf{r}_j$ with respect to the polarization state ϵ_j .

For the nonmagnetic crystal the atomic dipole-dipole resonant scattering is described by a symmetric second rank tensor f_{ij} containing the isotropic $f_{ij}^{iso} = f(E)\delta_{ij}$ and anisotropic f_{ij}^{an} parts that are solely defined by the atomic environment. f_{ij} can be reduced to a diagonal form with three different components in local axes, which can be thought as quantization axes. In arbitrary axes a symmetric second rank tensor has six different components, with six independent coefficients denoting three diagonal terms plus three Euler angles describing the rotation of the local axes to arbitrary axes. f_{ij}^{iso} contains only diagonal terms, but f_{ij}^{an} is a second rank tensor with zero trace, therefore, the number of its independent tensor components is five, because $f_{xx}^{an} + f_{yy}^{an} + f_{zz}^{an} = 0$. Only f_{ij}^{an} depends on polarizations and provides the forbidden reflection appearance. In the crystal axes, the resonant atomic factors may be not diagonal and may be different for crystallographically equivalent atoms. If the atomic environment is cubic, the electronic p states are degenerate and in the local axes all diagonal tensor components are equal to each other, therefore $f_{xx}^{an} = f_{yy}^{an} = f_{zz}^{an} = 0$. In a tetragonal environment $f_{xx}^{an} = f_{yy}^{an} \neq f_{zz}^{an}$, so that its diagonal components reflect the degree of electronic states degeneration. Off-diagonal components of the f_{ij} appear only when the local axes do not coincide with the crystal axes, so studying these components can provide valuable information about the directions of the local axes and about degeneration of electronic states. Since the off-diagonal tensor components are purely anisotropic, we will omit the superscript below.

3. Symmetry Consideration for TeO₂

Paratellurite TeO₂ is described by the space group $P4_12_12$ (or $P4_32_12$) with lattice parameters $a = 4.8082 \text{ \AA}$ and $c = 7.612 \text{ \AA}$ [30]. Te atoms occupy the Wyckoff position 4(a) (with $x = y = 0.02689$), O atoms occupy the general Wyckoff position ($x = 0.2579, y = 0.1386, z = 0.1862$). Due to the screw axes 4_1 and 2_1 the reflections $h00$ with $h = 2n$ and $00l$ with $l = 4n$ are allowed [31]. The unit cell of TeO₂ is shown in Figure 1.

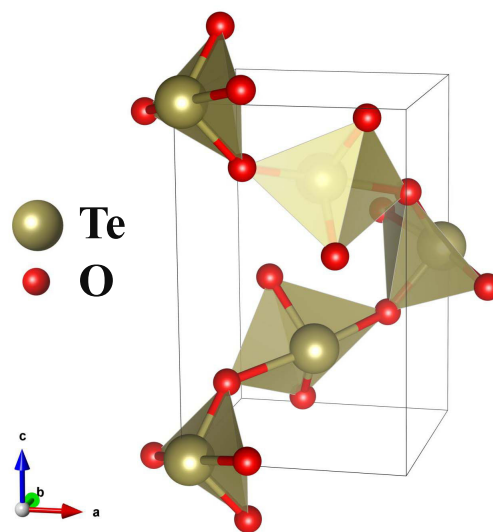


Figure 1. Unit cell of TeO₂. Big yellow balls are tellurium atoms, small red balls are oxygen atoms.

Let us consider the resonant structure factors, corresponding to the forbidden reflections $h00$ with $h = 2n + 1$ and $00l$ with $l = 4n + 2$. Assuming the dipole-dipole approximation, resonance scattering by Te atoms is described by symmetric (by permutation of indices) tensor of the second rank. Symmetry of the atomic position implies restrictions on the number of independent tensor components [32]. Te atoms lie on the two-fold axes placed between the **a** and **b** crystal axes, which gives us $f_{xx} = f_{yy}$, $f_{xz} = -f_{yz}$. The structure factor is a sum of atomic scattering factors of all atoms in a unit cell taking into account the rotation of the tensor axes under the symmetry elements of the space group $\hat{g}_s = (\hat{R}_s | \tau_s)$:

$$\hat{F}(\mathbf{H}) = \sum_s \hat{R}_s \hat{f}^1 \hat{R}_s^{-1} \exp 2\pi i \mathbf{H}(\hat{R}_s \mathbf{r}_1 + \tau_s), \quad (6)$$

where \hat{R}_s is the rotational part of the symmetry operation, τ_s is the corresponding fractional translation, \hat{f}^1 is the atomic scattering factor tensor of the atom with coordinates \mathbf{r}_1 within a Wyckoff position. The atomic tensor factors describing the dipole-dipole resonant scattering by Te atoms are equal to:

$$f_{ij}(\text{Te1}) = \begin{pmatrix} f_{xx} & f_{xy} & f_{xz} \\ f_{xy} & f_{xx} & -f_{xz} \\ f_{xz} & -f_{xz} & f_{zz} \end{pmatrix}. \quad (7)$$

$$f_{ij}(\text{Te2}) = \begin{pmatrix} f_{xx} & -f_{xy} & f_{xz} \\ -f_{xy} & f_{xx} & f_{xz} \\ f_{xz} & f_{xz} & f_{zz} \end{pmatrix}. \quad (8)$$

$$f_{ij}(\text{Te3}) = \begin{pmatrix} f_{xx} & f_{xy} & -f_{xz} \\ f_{xy} & f_{xx} & f_{xz} \\ -f_{xz} & f_{xz} & f_{zz} \end{pmatrix}. \quad (9)$$

$$f_{ij}(\text{Te4}) = \begin{pmatrix} f_{xx} & -f_{xy} & -f_{xz} \\ -f_{xy} & f_{xx} & -f_{xz} \\ -f_{xz} & -f_{xz} & f_{zz} \end{pmatrix}. \quad (10)$$

The following tensor describes the forbidden reflection $h00$ with $h = 2n + 1$ in the dipole-dipole resonant scattering:

$$\begin{aligned} F_{ij}(h00) &\sim \exp(2\pi i h x)(f_{ij}(\text{Te1}) - f_{ij}(\text{Te4})) + \exp(-2\pi i h x)(f_{ij}(\text{Te3}) - f_{ij}(\text{Te2})) = \\ &= 4 \begin{pmatrix} 0 & f_{xy} \cos(2\pi h x) & i f_{xz} \sin(2\pi h x) \\ f_{xy} \cos(2\pi h x) & 0 & 0 \\ i f_{xz} \sin(2\pi h x) & 0 & 0 \end{pmatrix}. \end{aligned} \quad (11)$$

For the $00l$ reflection with $l = 4n + 2$:

$$F_{ij}(00l) \sim (f_{ij}(\text{Te1}) - f_{ij}(\text{Te2}) + f_{ij}(\text{Te3}) - f_{ij}(\text{Te4})) = 4 \begin{pmatrix} 0 & f_{xy} & 0 \\ f_{xy} & 0 & 0 \\ 0 & 0 & 0 \end{pmatrix}. \quad (12)$$

The scattering amplitude is actually a 2-dimensional matrix, obtained through the 3-dimensional tensor \hat{F} taken between polarization vectors of the incident α and scattered β radiation:

$$F_{\beta\alpha} = \epsilon_{\beta}^* \hat{F} \epsilon_{\alpha}. \quad (13)$$

The off-diagonal terms in (14) may be non-zero in resonant scattering, contrary to the Thomson scattering case.

If the polarizations are linear we have in the basis σ, π

$$(F_{\beta\alpha}) = \begin{pmatrix} F_{\sigma\sigma} & F_{\sigma\pi'} \\ F_{\pi\sigma} & F_{\pi\pi'} \end{pmatrix}. \quad (14)$$

For the $00l$ reflections the polarization vectors are: $\mathbf{e}_\sigma = (\cos \phi, \sin \phi, 0)$, $\mathbf{e}_\pi = (-\sin \phi \sin \theta, \cos \phi \sin \theta, \cos \theta)$, $\mathbf{e}'_\pi = (\sin \phi \sin \theta, -\cos \phi \sin \theta, \cos \theta)$, where ϕ is the azimuthal angle, describing the rotation around the \mathbf{c} crystal axis, θ is the Bragg angle. When $\phi = 0$ \mathbf{e}_σ is parallel to the \mathbf{a} crystal axis. So, the structure amplitude $F_{\beta\alpha}(00l)$ is equal to:

$$F_{\beta\alpha}(00l) = 4f_{xy} \begin{pmatrix} \sin 2\phi & -\cos 2\phi \sin \theta \\ \cos 2\phi \sin \theta & \sin 2\phi \sin^2 \theta \end{pmatrix}. \quad (15)$$

For the $h00$ reflection the polarization vectors are: $\mathbf{e}_\sigma = (0, \cos \psi, \sin \psi)$, $\mathbf{e}_\pi = (\cos \theta_1, -\sin \psi \sin \theta_1, \cos \psi \sin \theta_1)$, $\mathbf{e}'_\pi = (\cos \theta_1, \sin \psi \sin \theta_1, -\cos \psi \sin \theta_1)$, where ψ is the azimuthal angle, θ_1 is the Bragg angle. When $\psi = 0$ \mathbf{e}_σ is parallel to the \mathbf{b} crystal axis. So, the structure amplitude $F_{\beta\alpha}(h00)$ is equal to:

$$F_{\beta\alpha}(h00) = 4 \cos \theta_1 \begin{pmatrix} 0 & f_{xy} \cos(2\pi hx) \cos \psi + if_{xz} \sin \psi \sin(2\pi hx) \\ f_{xy} \cos(2\pi hx) \cos \psi + if_{xz} \sin \psi \sin(2\pi hx) & 0 \end{pmatrix}. \quad (16)$$

Comparison of the expressions (16) and (15) shows that in the forbidden reflection $00l$ polarization of the incident radiation may change or not change depending on the azimuthal angle. For the $h00$ reflection σ polarization always changes during the scattering.

If the incoming beam is σ -polarized, the azimuthal dependence of the $00l$ reflection is a four-fold curve described by:

$$I_\sigma(00l, l = 4n + 2) \sim |f_{xy}|^2 (1 - \cos^2 2\phi \cos^2 \theta). \quad (17)$$

We see that the intensity is maximal at $\phi = \frac{\pi}{4} \pm \frac{\pi}{2}n$ (n is integer). If the incident radiation is σ -polarized, at this angle the outgoing radiation is also σ polarized, hence the polarization does not change.

For a $h00$ reflection we can write the following:

$$I_\sigma(h00, h = 2n + 1) \sim \cos^2 \theta_1 [\cos^2(2\pi hx) |f_{xy}|^2 \cos^2 \psi + \sin^2(2\pi hx) |f_{xz}|^2 \sin^2 \psi] \quad (18)$$

The azimuthal dependence of the $h00$ reflections integrated intensity is described by the two-fold function. This follows from (18) that at $\psi = 0$: $I(h00) \sim \cos^2(2\pi hx) |f_{xy}|^2$; but at $\psi = \frac{\pi}{2}$: $I(h00) \sim \sin^2(2\pi hx) |f_{xz}|^2$. Hence, from the ratio of the $h00$ reflection intensity at various azimuthal angles it is possible to determine the ratio between the tensor components as:

$$\frac{I(100, \psi = 0)}{I(100, \psi = \frac{\pi}{2})} = \frac{1}{\tan^2(2\pi hx)} \frac{|f_{xy}|^2}{|f_{xz}|^2}. \quad (19)$$

The presence of the off-diagonal tensor components means that the axes of local anisotropy do not coincide with the crystal axes. In the opposite case they turn out to be zero. At the L_1 absorption edge the electrons come from $1s$ to np excited states. In the crystal field, the p -states split into three sublevels p_x , p_y and p_z in the local anisotropy axes. The knowledge of the tensor f_{ij} components is important for the study of the electronic levels splitting. However, an experiment usually gives information only in arbitrary units. Determining the absolute values requires comparison with a previously known value, as it was done in [33], or with ab initio calculations.

4. Experimental

Paratellurite single crystals were grown by the Czochralski method. Two samples were prepared in the form of the plates with the sizes of $2 \times 2 \times 3 \text{ mm}^3$, one with the surface parallel to (001) plane, the other with the surface parallel to the (100) plane. The samples were polished and etched in 40% HF water solution. A good crystal quality was confirmed by the width of the Bragg reflection rocking curve very close to the theoretical values (FWHM = 7.0 arcsec for 004 and FWHM = 13.6 arcsec for 200).

The energy spectra of forbidden reflections in paratellurite were measured in two experiments with the photon energies close to the L_1 absorption edge ($E = 4938 \text{ eV}$). One experiment was carried out at the P23 beamline of PETRA III synchrotron radiation facility at DESY. The energy of photons was varied by the double-crystal monochromator. CRL-lenses were applied to collimate and focus the incidence beam on the sample to a spot with the size of about $50 \mu\text{m}$. Flat mirrors were used for harmonics rejection. The sample was mounted on a $5 + 2$ circle Huber goniometer.

The precise alignment of the angular orientation was made on allowed symmetrical Bragg reflections 004 ($\theta_B = 19.009^\circ$) and 200 ($\theta_B = 14.937^\circ$) measured at a non-resonant energy 10 keV. After that, the incident radiation energy was set to 4.938 keV close to the L_1 -edge of Te. For both 002 and 100 forbidden reflections, the azimuthal dependence (ψ -scan) and energy spectrum (E -scan) were measured. The azimuthal dependence for the 002 reflection revealed a well pronounced four-fold symmetry and was used to determine the position with maximum intensity suitable for the study of the energy spectrum. Also it allowed to choose the interval of azimuthal angles where Renninger multiple beam reflections are absent. The 100 forbidden reflection energy spectrum was also measured at the maximum azimuthal intensity. The experimental geometry corresponding to both experiments is shown in Figure 2.

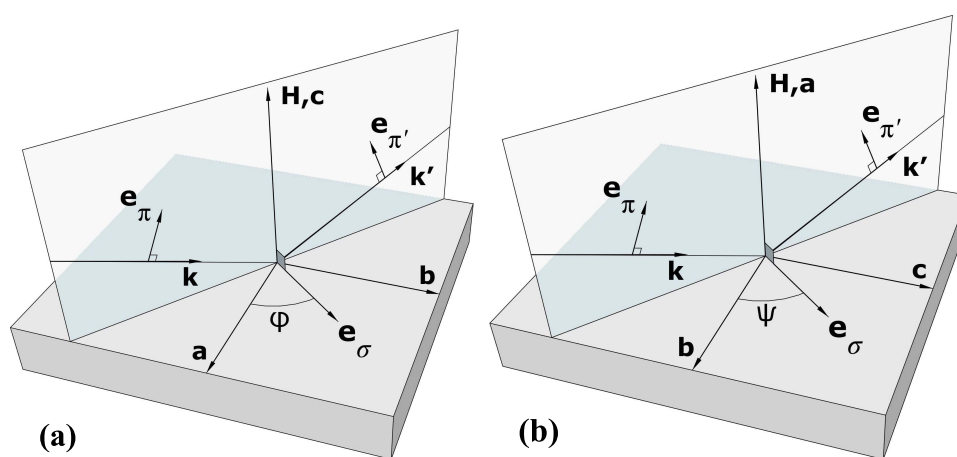


Figure 2. Left panel: (a) experimental geometry corresponding to the 002; right panel: (b) experimental geometry for the study of the 100 reflection.

Surprisingly the energy spectrum of the 100 reflection turned out to be very similar to that of the 002 reflection. This result was unexpected, because in accordance with theoretical considerations the energy spectrum of the 100 reflection has to be determined by two tensor components, and not only one single as in the case of the 002 spectrum.

To clarify the situation, the 002 forbidden reflection energy spectrum and its azimuthal dependence were repeatedly measured at the Kurchatov synchrotron radiation facility (Figure 3). The measurements were carried out at the beamline PHASE with a bending magnet source. The synchrotron beam was collimated by a parabolic mirror. The energy of photons was varied by the Si (111) double-crystal monochromator. The sagittal bend of the second crystal was used to focus the radiation in the horizontal plane. The sample was mounted on the 6-axis Huber goniometer. In this experiment the density of photon flux was much smaller than in the experiment at PETRA. The

results of the three measurements are shown in Figure 4. Because in different experiments the photon flux, exposition time and other conditions were not equivalent, it is difficult to directly compare the measured values. So, we have scaled the spectra shown in the Figure 4 with reference to the post-edge region above the white line. One can see that the energy spectra of the 002 reflection measured at the PETRA III and Kurchatov synchrotron radiation facility completely coincide. The spectrum of the 100 reflection looks almost the same as 002, but we cannot be sure that the absolute scaling is correct. Therefore, numerical calculations of both reflection were made and the results are represented in the next section.

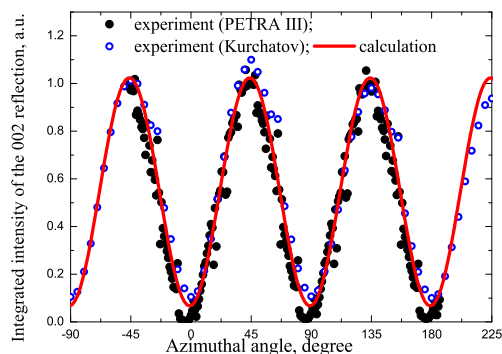


Figure 3. Azimuthal dependence of the 002 reflection, measured at PETRA III (black points), Kurchatov synchrotron radiation source (open blue points) and calculation at $E = 4938$ eV.

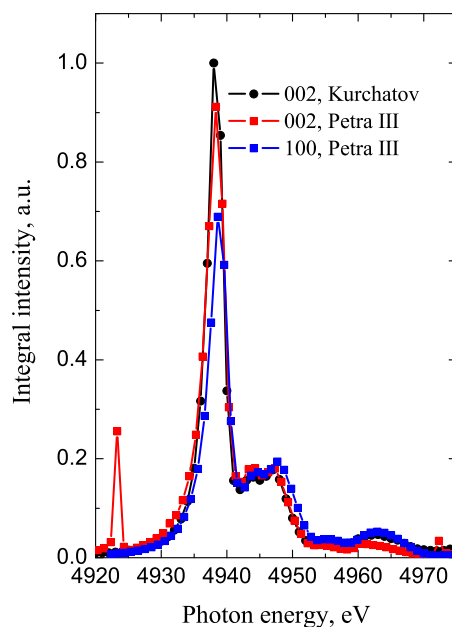


Figure 4. Experimentally measured energy spectra of the forbidden reflections: 002 spectrum measured at the Kurchatov synchrotron (black); 002 spectrum measured at PETRA III (red); 100 spectrum measured at PETRA III (blue).

5. Results and Discussion

The energy spectra, absorption coefficients, as well as azimuthal dependencies of the 100 and 002 forbidden reflections were calculated using the FDMNES ab initio code [34–36]. The similarity of the 002 and 100 energy spectra was unexpected, since theoretical consideration have shown that the 002 reflection is provided only by the tensor component f_{xy} , but two tensor components f_{xy} and f_{xz} contribute to the 100 reflection. To clarify this finding we made the calculation of the azimuthal dependence of the 100 reflection and corresponding tensor components. They are shown in the Figures 5 and 6.

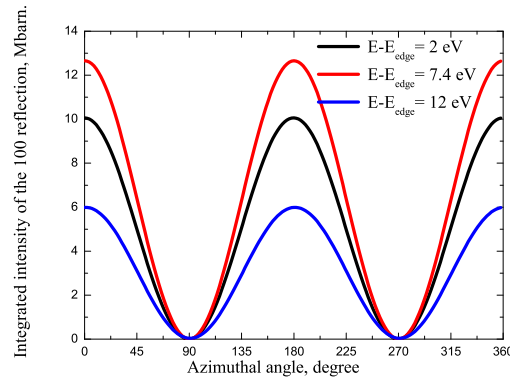


Figure 5. Azimuthal dependence of the 100 reflection at $\Delta E = 2$ eV (black), 7.4 eV (red) and 12 eV (blue), from ab initio calculations.

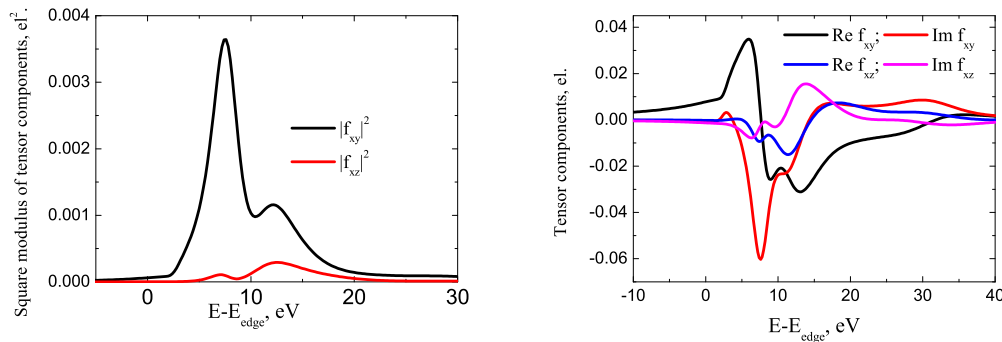


Figure 6. Left panel (a): calculated energy dependence of the square modulus of the two tensor components $|f_{xy}|^2$ (black) and $|f_{xz}|^2$ (red); right panel (b): calculated real and imaginary parts of the tensor components f_{xy} and f_{xz} .

The right panel of Figure 6 shows the real and imaginary parts of the tensor components f_{xy} and f_{xz} and the left panel of Figure 6 shows the square of the tensor components modulus. We can see from the Figure 6 that the component f_{xz} is smaller than f_{xy} , but not significantly. However, the contribution of $|f_{xz}|^2$ to the 100 spectrum is negligible due to the coefficient $\frac{1}{\tan^2(2\pi h x)}$, which is equal to 1/35 for the 100 reflection. For this reason, the energy spectrum of this reflection is almost completely determined by the component f_{xy} , which results in its spectral shape very similarly to that of 002. The ratio of the tensor components agrees well with the results, which can be obtained from the azimuthal dependence shown in Figure 6. This demonstrates the possibilities to determine the ratio of the tensor components directly from the experimental data.

Now we can compare the integrated intensities of the 002 and 100 reflection measured at azimuthal angles in maxima as following:

$$\frac{I(002)}{I(100)} = \frac{1}{\cos^2(2\pi hx) \cos^2 \theta_1}. \quad (20)$$

Taking $\theta = 19.3^\circ$, $\theta_1 = 15.1^\circ$ we obtain this ratio ~ 1.1 . It shows that the integrated intensities of both reflections are almost equal to each other. It is also worth considering the influence of linear dichroism on the spectral shape of both reflections. In a tetragonal crystal resonant part of absorption is described by two coefficients μ_0 and μ_a , so that [37]:

$$\mu(E, \alpha) = \mu_{nonres} + \mu_0(E) - \frac{3 \cos^2 \alpha - 1}{\sqrt{2}} \mu_a(E), \quad (21)$$

where $\mu_{nonres}(E)$ is an absorption due to the processes other than the considered absorption edge, $\mu_0(E)$ is an isotropic part of resonant absorption, $\mu_a(E)$ is its anisotropic part and α is the angle between the polarization vector and the four-fold axis. For the case of the polarization vector perpendicular to the *c* axis we have:

$$\mu_{par}(E) = \mu_{nonres} + \mu_0(E) + \frac{1}{\sqrt{2}} \mu_a(E), \quad (22)$$

when the polarization vector is parallel to the *c* axis:

$$\mu_{perp}(E) = \mu_{nonres} + \mu_0(E) - \sqrt{2} \mu_a(E). \quad (23)$$

Usually the absorption is measured in an experiment through the X-ray fluorescence yield simultaneously with Bragg reflections. However, for the L_1 absorption in Te the fluorescence channel is very weak. Therefore, the absorption coefficients corresponding to the polarization vectors parallel and perpendicular to the *c* axis were calculated with the help of the FDMNES code together with the energy spectra of the 100 and 002 reflections. They are shown in Figure 7 and demonstrate the existence of linear dichroism.

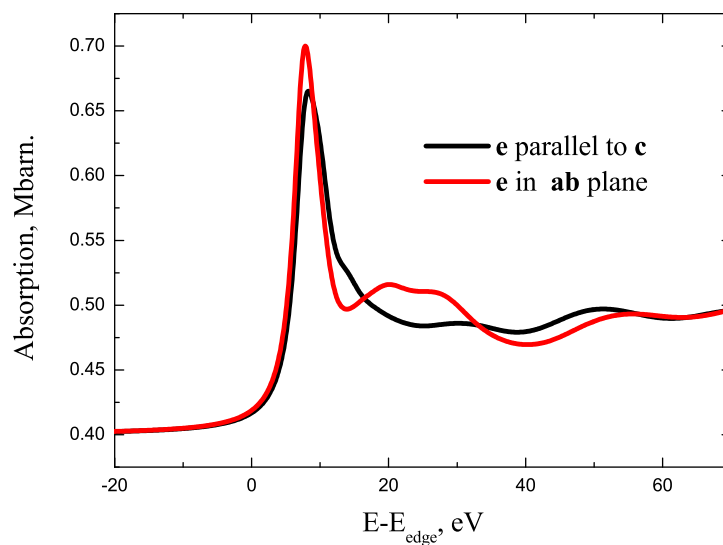


Figure 7. Absorption coefficients of X-rays with polarization parallel (black) and perpendicular (red) to the *c* crystal axis.

Looking at the experimental scheme shown in Figure 2 we see that the maximum of the 002 spectra corresponds to the $\sigma \rightarrow \sigma$ scattering channel, hence we can use μ_{perp} for the calculation. The maximum of the 100 reflection intensity is reached in $\sigma \rightarrow \pi$ scattering when $\psi = 0$, the σ polarization of the incoming wave is parallel to the **b** crystal axis, and the angle between the π polarization of the outgoing wave and the **a** axis is θ_1 . As $\theta_1 = 19^\circ$ we can suppose approximately that $\mathbf{e}'_\pi \parallel \mathbf{a}$, hence we also use μ_{perp} as absorption coefficient.

The energy spectra of the 100 and 002 reflection were calculated with the help of the FDMNES code. The calculations were made with the multiple scattering mode involving 119 atoms and show satisfactory fitting of the experimental data. The results of the 002 energy spectrum calculation in comparison with the experimental data is shown in Figure 8.

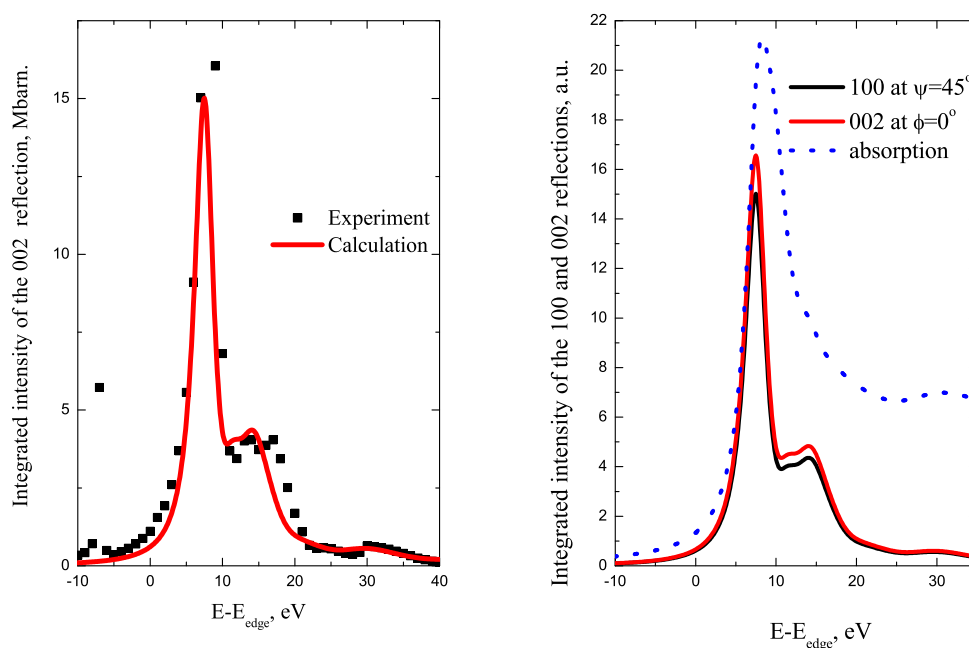


Figure 8. Left panel: calculated energy spectrum of the 002 reflection in comparison with experimental data; right panel: calculated 002 and 100 reflections energy spectra (in maximum azimuthal intensity).

The calculated energy spectra of the 100 and 002 reflections are shown in Figure 6. The calculations reveal that the energy spectra are identical and the scaling factor of 1.1 is in a good agreement with theoretical predictions. The absorption spectrum corresponding to μ_{perp} is shown only to demonstrate the position of the forbidden reflections on the energy scale.

In summary, the calculations on the one hand allow to account for the correct absorption and on the other hand explain the experimentally observed scaling of both forbidden reflections.

6. Conclusions

The study of the energy, azimuthal, and polarization dependency of forbidden reflections provides valuable information on the electronic structure and the local environment of atoms in crystals. Resonant atomic factors corresponding to dipole-dipole transitions near the L_1 absorption edge are described by a symmetric second-rank tensor whose diagonal components in the local coordinate axes reflect the splitting of the p electronic states. The off-diagonal tensor components depend on the Euler angles between the local and crystalline axes. It is shown that measuring the azimuthal dependence of forbidden reflections in paratellurite TeO_2 allows to obtain information on the ratio of off-diagonal

tensor components directly from the experimental data. The energy dependence of the forbidden reflections also gives access to the spectral shape of the tensor components. However, it is necessary to carefully choose the Bragg reflections, since the contributions of tensor components differs for different reflections. We examined the reflections $00l, l = 4n + 2$ and $h00, h = 2n + 1$ in paratellurite. The former appears due to the tensor component f_{xy} , the latter is caused by two tensor components f_{xy} and f_{xz} . Two representative reflections of these types, namely the 002 and 100 reflections, were measured on two sources of synchrotron radiation. By analyzing the integrated intensity of the 100 reflection at various azimuthal angles, we have determined the ratio between the components of the structural tensor factor $|F_{xz}/F_{xy}|$, which is small for reflection 100. The energy dependence of the component f_{xz} cannot be extracted from the energy spectrum of the 100 reflection, but its contribution is approximately 12 times stronger for reflection 300 and will be measured directly in future experiments. Meanwhile, all off-diagonal components of the dipole-dipole resonant atomic form factor of Te can be determined at the maximum of the energy spectrum out of the azimuthal scan of the 100 reflection. This will allow to determine the Euler angles between the local quantization axes and the crystal axes. Such information cannot be obtained from the conventional X-ray absorption spectroscopies.

The phenomenological findings were confirmed by ab initio calculations. They showed that although the tensor component f_{xz} is not small compared to the component f_{xy} , its contribution to the integrated reflection intensity 100 is negligible due to specific geometric factors, so that the energy spectra of the 100 and 002 reflections are described by the same tensor component f_{xy} . We also found that, despite of the presence of linear dichroism in absorption, it does not affect the spectral shape of the forbidden reflections.

In addition, we demonstrated that numerical calculations also make it possible to compare and combine experimental results obtained at different synchrotron radiation sources.

In principle, the reflection intensity is proportional to the number of detected photons, whereas the results are usually expressed in arbitrary units. This makes it difficult to compare data obtained under different conditions or on different equipment. To solve this scaling issue of absolute intensities, it is necessary to attach calculations that are made on an absolute scale. When the adjustment of the experimental results is done, these means allow us to find the correct scaling factor between data sets, which were measured on different equipment.

Author Contributions: Conceptualization, V.D., E.O. and D.N.; methodology, E.O.; software, A.O., K.K.; validation, M.Z.; formal analysis, E.O.; investigation, D.N., E.M., M.B., A.K. (Anton Kulikov), A.K. (Azat Khadiev) and A.P.; resources, N.M. and A.B.; writing—original draft preparation, E.O.; writing—review and editing, V.D., D.N. and M.Z.; visualization, K.K.; supervision, Y.P.; project administration, A.B., N.M. All authors have read and agreed to the published version of the manuscript.

Funding: This research was funded by the Russian Foundation for Basic Research (project no. 19-52-12029, study of the forbidden Bragg reflections, and project no. 19-02-00483, calculation of the Renninger reflections positions).

Acknowledgments: V.D. was partly supported by the Ministry of Science and Higher Education over a state contract for the Federal Research Center Crystallography and Photonics, Russian Academy of Sciences. Parts of this calculations were carried out using the equipment of the shared research facilities of HPC computing resources at Lomonosov Moscow State University [38]. We acknowledge DESY (Hamburg, Germany), a member of the Helmholtz Association HGF, for the provision of experimental facilities.

Conflicts of Interest: The authors declare no conflict of interest.

Abbreviations

The following abbreviations are used in this manuscript:

PETRA	Photonics Electronics Technology Research Association
DAFS	Diffraction Anomalous Fine Structure
FWHM	Full Width Half Maximum
CRL-lenses	Compound Refractive Lens

References

1. Zschornak, M.; Richter, C.; Nentwich, M.; Stöcker, H.; Gemming, S.; Meyer, D.C. Probing a crystal's short-range structure and local orbitals by Resonant X-ray Diffraction methods. *Cryst. Res. Technol.* **2014**, *49*, 43–54. [\[CrossRef\]](#)
2. Dmitrienko, V.E. Forbidden reflections due to anisotropic X-ray susceptibility of crystals. *Acta Crystallogr. Sect. A* **1983**, *39*, 29–35. [\[CrossRef\]](#)
3. Templeton, D.H.; Templeton, L.K. X-ray dichroism and polarized anomalous scattering. *Acta Crystallogr. Sect. A Found. Crystallogr.* **1981**, *37*, C309. [\[CrossRef\]](#)
4. Templeton, D.H.; Templeton, L.K. X-ray Birefringence and Forbidden Reflections in Sodium Bromate. *Acta Cryst.* **1986**, *A42*, 478–481. [\[CrossRef\]](#)
5. Hodeau, J.L.; Favre-Nicolin, V.; Bos, S.; Renevier, H.; Lorenzo, E.; Berar, J.F. Resonant diffraction. *Chem. Rev.* **2001**, *101*, 1843–1867. [\[CrossRef\]](#) [\[PubMed\]](#)
6. Dmitrienko, V.E.; Ishida, K.; Kirfel, A.; Ovchinnikova, E.N. Polarization anisotropy of R-ray atomic factors and 'forbidden' resonant reflections. *Acta Crystallogr. Sect. A Found. Crystallogr.* **2005**, *61*, 481–493. [\[CrossRef\]](#)
7. Bohnenbuck, B.; Zegkinoglou, I.; Stremper, J.; Nelson, C.S.; Wu, H.H.; Schüßler-Langeheine, C.; Reehuis, M.; Schierle, E.; Leininger, P.; Herrmannsdörfer, T.; et al. Magnetic structure of $\text{RuSr}_2\text{GdCu}_2\text{O}_8$ determined by resonant X-ray diffraction. *Phys. Rev. Lett.* **2009**, *102*, 1–4. [\[CrossRef\]](#) [\[PubMed\]](#)
8. Paolasini, L. Resonant and magnetic X-ray diffraction by polarized synchrotron radiation. *École Thématique Société Française Neutron.* **2014**, *13*, 03002. [\[CrossRef\]](#)
9. Hatton, P.D.; Johnson, R.D.; Bland, S.R.; Mazzoli, C.; Beale, T.A.; Du, C.H.; Wilkins, S.B. Magnetic structure determination using polarised resonant X-ray scattering. *J. Magn. Magn. Mater.* **2009**, *321*, 810–813. [\[CrossRef\]](#)
10. Zimmermann, M.; Nelson, C.S.; Hill, J.P.; Gibbs, D.; Blume, M.; Casa, D.; Keimer, B.; Murakami, Y.; Kao, C.C.; Venkataraman, C.; et al. X-ray resonant scattering studies of orbital and charge ordering in $\text{Pr}_{1-x}\text{Ca}_x\text{MnO}_3$. *Phys. Rev. B* **2001**. [\[CrossRef\]](#)
11. Murakami, Y.; Kawada, H.; Kawata, H.; Tanaka, M.; Arima, T.; Moritomo, Y.; Tokura, Y. Direct observation of charge and orbital ordering in $\text{La}_{0.5}\text{Sr}_{1.5}\text{MnO}_4$. *Phys. Rev. Lett.* **1998**, *80*, 1932–1935. [\[CrossRef\]](#)
12. Dmitrienko, V.E.; Ovchinnikova, E.N. Chirality-induced 'forbidden' reflections in R-ray resonant scattering. *Acta Crystallogr. Sect. A* **2001**, *57*, 642–648. [\[CrossRef\]](#) [\[PubMed\]](#)
13. di Matteo, S.; Joly, Y.; Bombardi, A.; Paolasini, L.; de Bergevin, F.; Natoli, C.R. Local chiral-symmetry breaking in globally centrosymmetric crystals. *Phys. Rev. Lett.* **2003**, *91*, 1–4. [\[CrossRef\]](#) [\[PubMed\]](#)
14. Kokubun, J.; Kanazawa, M.; Ishida, K.; Dmitrienko, V.E. Temperature-induced distortions of electronic states observed via forbidden Bragg reflections in germanium. *Phys. Rev. B—Condens. Matter Mater. Phys.* **2001**, *64*, 732031–732034. [\[CrossRef\]](#)
15. Collins, P.; Laundry, D.; Dmitrienko, E.; Mannix, D.; Thompson, P. Temperature-dependent forbidden resonant R-ray scattering in zinc oxide. *Phys. Rev. B—Condens. Matter Mater. Phys.* **2003**, *68*, 1–4. [\[CrossRef\]](#)
16. Richter, C.; Novikov, D.V.; Mukhamedzhanov, E.K.; Borisov, M.M.; Akimova, K.A.; Ovchinnikova, E.N.; Oreshko, A.P.; Stremper, J.; Zschornak, M.; Mehner, E.; et al. Mechanisms of the paraelectric to ferroelectric phase transition in RbH_2O_4 probed by purely resonant R-ray diffraction. *Phys. Rev. B—Condens. Matter Mater. Phys.* **2014**, *89*, 1–9. [\[CrossRef\]](#)
17. Beutier, G.; Collins, S.P.; Nisbet, G.; Akimova, K.A.; Ovchinnikova, E.N.; Oreshko, A.P.; Dmitrienko, V.E. Proton configurations in the hydrogen bonds of KH_2PO_4 as seen by resonant R-ray diffraction. *Phys. Rev. B—Condens. Matter Mater. Phys.* **2015**, *92*, 1–11. [\[CrossRef\]](#)
18. Gorfman, S.; Tsirelson, V.; Pucher, A.; Morgenroth, W.; Pietsch, U. X-ray diffraction by a crystal in a permanent external electric field: Electric-field-induced structural response in $\alpha\text{-GaPO}_4$. *Acta Crystallogr. Sect. A Found. Crystallogr.* **2006**, *62*, 1–10. [\[CrossRef\]](#)
19. Gorfman, S.; Schmidt, O.; Tsirelson, V.; Ziolkowski, M.; Pietsch, U. Crystallography under external electric field. *Z. Anorg. Allg. Chem.* **2013**, *639*, 1953–1962. [\[CrossRef\]](#)
20. van Reeuwijk, S.J.; Puig-Molina, A.; Graafsma, H. Electric-field-induced structural changes in KH_2PO_4 at room temperature and at 167 K. *Phys. Rev. B Condens. Matter Mater. Phys.* **2001**, *64*, 18–20. [\[CrossRef\]](#)

21. Richter, C.; Zschornak, M.; Novikov, D.; Mehner, E.; Nentwich, M.; Hanzig, J.; Gorfman, S.; Meyer, D.C. Picometer polar atomic displacements in strontium titanate determined by resonant X-ray diffraction. *Nat. Commun.* **2018**, *9*, 1–9. [CrossRef] [PubMed]
22. Kovalchuk, M.V.; Blagov, A.E.; Kulikov, A.G.; Marchenkov, N.V.; Pisarevsky, Y.V. Formation of unusual nonferroic domains in TeO₂ single crystals under external electric field. *Crystallogr. Rep.* **2014**, *59*, 862–866. [CrossRef]
23. Kulikov, A.G.; Blagov, A.E.; Marchenkov, N.V.; Lomonov, V.A.; Vinogradov, A.V.; Pisarevsky, Y.V.; Kovalchuk, M.V. Rearrangement of the Structure of Paratellurite Crystals in a Near-Surface Layer Caused by the Migration of Charge Carriers in an External Electric Field. *JETP Lett.* **2018**, *107*, 646–650. [CrossRef]
24. Kulikov, A.G.; Pisarevskii, Y.V.; Blagov, A.E.; Marchenkov, N.V.; Lomonov, V.A.; Petrenko, A.A.; Kovalchuk, M.V. Variation of a Defect Structure of Lithium Tetraborate (Li₂B₄O₇) in an External Electric Field. *Phys. Solid State* **2019**, *61*, 548–554. [CrossRef]
25. Kulikov, A.G.; Blagov, A.E.; Ilin, A.S.; Marchenkov, N.V.; Pisarevskii, Y.V.; Kovalchuk, M.V. Anisotropy and kinetics of the migration-induced layer formation in TeO₂. *J. Appl. Phys.* **2020**, *127*. [CrossRef]
26. Blume, M. Magnetic effects in anomalous dispersion. In *Resonant Anomalous X-ray Scattering*; Materlik, G., Ed.; Elsevier: Amsterdam, The Netherlands, 1994; p. 495.
27. Maslen, E.N. X-ray absorption. In *International Tables for Crystallography*; Springer: Berlin/Heidelberg, Germany, 2006; Volume C, pp. 599–608.
28. Belyakov, V.A. Diffraction of mössbauer gamma rays in crystals. *Sov. Phys.—Uspekhi* **1975**, *18*, 267–291. [CrossRef]
29. Hannon, J.; Trammell, G. Mossbauer Diffraction. II. Dynamical Theory of Mossbauer Optics. *Phys. Rev.* **1969**, *186*, 306–325. [CrossRef]
30. Thomas, P.A. The crystal structure and absolute optical chirality of paratellurite, α -teo₂. *J. Phys. C Solid State Phys.* **1988**, *21*, 4611–4627. [CrossRef]
31. Hahn, T. *International Tables for Crystallography*; Springer: Berlin/Heidelberg, Germany, 2005.
32. Sirotna, Y.; Shaskolskaia, M.P. *Fundamentals of Crystal Physics*; MIR Publishers: Moscow, Russia, 1982.
33. Mukhamedzhanov, E.K.; Borisov, M.M.; Morkovin, A.N.; Antonenko, A.A.; Oreshko, A.P.; Ovchinnikova, E.N.; Dmitrienko, V.E. Absolute intensity and phase of the resonant X-ray scattering from a germanium crystal. *JETP Lett.* **2008**, *86*, 783–787. [CrossRef]
34. Joly, Y.; Matteo, S.D.; Bunău, O. Resonant X-ray diffraction: Basic theoretical principles. *Eur. Phys. J. Spec. Top.* **2012**, *208*, 21–38. [CrossRef]
35. Joly, Y.; Collins, S.P.; Grenier, S.; Tolentino, H.C.; De Santis, M. Birefringence and polarization rotation in resonant R-ray diffraction. *Phys. Rev. B—Condens. Matter Mater. Phys.* **2012**, *86*, 1–4. [CrossRef]
36. Joly, Y. The FDMNES Project. Available online: <http://neel.cnrs.fr/spip.php?rubrique1007> (accessed on 18 August 2020).
37. Brouder, C. Angular dependence of X-ray absorption spectra. *J. Phys. Condens. Matter* **1990**, *2*, 701–738. [CrossRef]
38. Sadovnichy, V.; Tikhonravov, A.; Voevodin, V.; Opanasenko, V. “Lomonosov”: Supercomputing at Moscow State University. In *Contemporary High Performance Computing*; Vetter, J., Ed.; CRC Press: Boca Raton, FL, USA, 2013; pp. 283–307.

